Phase-Locked Rotation of Crystallized Non-neutral Plasmas by Rotating Electric Fields

X.-P. Huang, J.J. Bollinger, T.B. Mitchell, and Wayne M. Itano
Time & Frequency Division, National Institute of Standards and Technology, 325 Broadway, Boulder, CO 80303
(October 27, 1997)

We report the precise control of the rotation frequency of strongly coupled non-neutral plasmas by rotating electric fields. These plasmas of up to 10^6 $^9Be^+$ ions are trapped in a Penning trap and laser cooled into crystallized structures which undergo a rigid-body rotation. Bragg diffraction shows that the crystalline lattice can be stable for longer than 30 min ($\sim 10^8$ rotations), and that the plasma rotation can be phase locked to the applied field without any slip. These co-rotating plasmas are in a new kind of thermal equilibrium whose asymmetric surface shape (triaxial ellipsoid) has been measured.

PACS numbers: 32.80.Pj, 52.25.Wz

Large numbers of charged particles with a single sign of charge can be trapped and cooled in Penning traps [1,2], which use a combination of static electric and magnetic fields for particle confinement. The global rotation of these non-neutral plasmas about the magnetic field axis is necessary for the radial confinement [3]. Active control of this rotation prevents plasmas from spinning down under the ambient drag from static field errors and background neutrals, and is important for a number of experiments including Coulomb crystal studies [4,5], precision spectroscopy [6–8], measurements of particle and energy transport [9], trapping of anti-matter plasmas [10,11], and storage of highly stripped ions [12]. As an example, the second-order Doppler (time dilation) shift due to rotational velocity in a Penning trap atomic clock can be minimized by stabilizing the rotation at a particular frequency [7]. Radiation pressure from laser beams has been used to vary the plasma rotation frequency [13,14]. However, this method is limited to the few ion species whose atomic transitions are accessible by a laser, and is not precise due to laser power, frequency, and pointing fluctuations. Recently, rotating azimuthally asymmetric ("rotating wall") electric fields have been used to apply a torque on Mg^+ plasmas with temperatures ranging from 1 K to 5×10^4 K (4 eV), resulting in steady-state confinement and density compression [15,16]. For these uncorrelated plasmas, the stabilized rotation frequency is somewhat less than that of the rotating field, with a slip which increases with the plasma temperature.

In this letter, we demonstrate that "rotating wall" electric fields applied to a Penning trap with quadratic potentials can control the rotation of laser-cooled, crystallized $^9Be^+$ plasmas without slip, thus extending the applicability of this technique from uncorrelated plasmas to strongly coupled systems. Both rotating dipole and quadrupole fields perpendicular to the magnetic field are used to provide this precise control of the plasma rotation. We will concentrate on quadrupole field results, since the dipole configuration apparently requires multiple charged species or other non-ideal effects to be effective and is therefore less general. The rotating quadrupole field interacts with charges near the plasma surface, creating a small-amplitude traveling wave. The torque due to this wave is then transferred to the plasma interior through Coulomb interactions, which act to bring the plasma to the same rotation frequency as the applied field [17]. For temperatures up to ~ 10 K, side-view images show that the plasma shape, which is determined by the rotation frequency, can be varied by gradually changing the rotating field frequency. When the plasma is sufficiently cold and crystalline lattices are formed, Bragg diffraction provides a more accurate measurement of the rotation frequency. It is observed that the lattice and its orientation with respect to the axial laser beam can be stable for longer than 30 min ($\sim 10^8$ rotations), and its rotation can be phase locked to the rotating field during this time. In essence, these co-rotating plasmas have reached a new kind of global thermal equilibrium [17], where the rotation frequency (and hence the density) is precisely set by an external drive. We have observed the predicted triaxial ellipsoidal surface of this equilibrium state for oblate (pancake-like) plasmas.

Figure 1 shows the apparatus and the rotating quadrupole field. The trap consists of a 127 mm long stack of cylindrical electrodes at room-temperature with an inner diameter of 40.6 mm, enclosed in a 10^{-8} Pa vacuum chamber. The uniform magnetic field $B_0 = 4.46$ T is aligned parallel to the trap axis within 0.01°, giving a $^9Be^+$ (charge e and mass m) cyclotron frequency $\Omega = eB_0/m = 2\pi \times 7.61$ MHz. An axisymmetric trapping potential $(m\omega_z^2/2e)[z^2 - (x^2 + y^2)/2]$ is generated near the trap center by biasing the central electrodes to a negative voltage $-V_0$. At $V_0 = 1$ kV, the single-particle axial frequency $\omega_z = 2\pi \times 799$ kHz and the magnetron frequency $\omega_m = (\Omega - \sqrt{\Omega^2 - 2\omega_z^2})/2 = 2\pi \times 42.2$ kHz. The rotating quadrupole field, which has a potential $\propto (y^2 - x^2)\cos(2\omega_w t) + 2xy \sin(2\omega_w t)$, is generated by applying properly phased sinusoidal voltages of amplitude V_w to the 6-fold azimuthal sectors of the compensation electrodes [15].

We create $^9Be^+$ plasmas by ionizing neutral Be atoms

in a separate trap (not shown) and then transferring the ions to the main trap for experimentation [4,14]. This procedure can be repeated several times to accumulate up to 10^6 ions. Immediately after loading, less than 5 % are contaminant ions, but this fraction grows on a 20 hour timescale due to $^9Be^+$ reactions with neutrals forming ions with smaller charge-to-mass ratio. The trapped $^9Be^+$ ions are Doppler cooled by two laser beams at wavelength $\lambda \approx 313.11$ nm. From previous experiments [13,14], we estimate that temperatures $T \lesssim 10$ mK can be obtained. Here, $k_B T$ refers to the average ion thermal energy in a frame rotating with the plasma which is typically much smaller than the average kinetic energy in the global rotation ($\sim 10^2$ K). The axial cooling beam, directed parallel to $\mathbf{B_0}$, only cools the ion thermal motion while not affecting the global rotation. A second beam propagating perpendicular to $\mathbf{B_0}$ (not shown and turned off during the Bragg scattering measurements) is used to vary the rotation frequency.

When the cloud reaches thermal equilibrium at these cryogenic temperatures, it forms a uniform density spheroid, bounded by $z^2/z_0^2 + (x^2+y^2)/r_0^2 = 1$, with a rigid-body rotation frequency ω_r in the range $\omega_m < \omega_r < \Omega - \omega_m$ [14]. The particle density n_0 is determined from ω_r according to $\omega_p^2 \equiv e^2 n_0/\epsilon_0 m = 2\omega_r(\Omega - \omega_r)$, where ω_p is the plasma frequency [14]. Since the influence of image charges is negligible here, the effective trapping potential in the frame rotating with the plasma, (x_r, y_r, z), is $\Phi_r = (m\omega_z^2/2e)[z^2 + \beta(x_r^2 + y_r^2)]$, where radial trapping strength $\beta \equiv (\omega_p^2 - \omega_z^2)/2\omega_z^2 = \omega_r(\Omega - \omega_r)/\omega_z^2 - 1/2 > 0$ determines the aspect ratio $\alpha \equiv z_0/r_0$ [14,17]. An f/5 imaging system detects resonantly scattered photons from the axial cooling beam (diameter ≈ 0.4 mm, power $\approx 50\,\mu$W) to produce a side-view image of the $^9Be^+$ ions, from which we measure α to obtain ω_r and n_0.

For the typical condition of $T \lesssim 10$ mK and $n_0 \gtrsim 4 \times 10^8\,\mathrm{cm}^{-3}$, we obtain a Coulomb coupling parameter $\Gamma \equiv (e^2/4\pi\epsilon_0 a_{WS})(k_B T)^{-1} > 200$, where Wigner-Seitz radius a_{WS} is defined by $4\pi a_{WS}^3/3 \equiv n_0^{-1}$. The strong ion-ion coupling results in the formation of crystalline lattices, which are typically body-centered cubic (bcc), in nearly spherical plasmas ($\alpha \approx 1$) with ion number $N \gtrsim 2 \times 10^5$ [4,5]. As shown in Fig. 1, Bragg-scattered light from the axial cooling beam is detected with a second camera near the forward-scattering direction since $\lambda \ll a_{WS}$ [4].

When the rotating fields are first applied, their frequency ω_w is set close to ω_r so that they interact strongly with the plasma. By measuring the photon scattering rate from the cooling beam for a fixed laser frequency, we observe that the ion temperature does not change significantly with the application of the rotating fields. Since the rotating quadrupole field typically causes less than 1 % shape distortion to the plasma (see later discussions), ω_r can still be inferred from aspect ratio α within the 5 % uncertainty of the method. With V_w sufficiently large, we are able to vary ω_r by gradually changing ω_w. By tuning the laser frequency far below the resonance or blocking the laser for short periods of time (~ 1 min), we can increase T up to ~ 10 K such that the plasma is weakly correlated ($\Gamma \approx 0.2$ for $n_0 \approx 4 \times 10^8\,\mathrm{cm}^{-3}$), and still be able to control ω_r. Figure 2 shows ω_r versus ω_w for several plasmas with $N < 7 \times 10^4$ and $\omega_r \ll \Omega/2$ ($\omega_r = \Omega/2$ is the Brillouin flow with maximal density $n_B = 5.9 \times 10^9\,\mathrm{cm}^{-3}$). The plasma rotation frequency ω_r tracks ω_w closely within the experimental accuracy, demonstrating external control of the plasma rotation by the rotating quadrupole field with both weak and strong Coulomb coupling.

For a more accurate determination of ω_r, we detect the time dependence of Bragg-scattered light from rotating crystals by strobing the diffraction camera with a gateable image intensifier [4,5]. Figure 3(a) shows a time-averaged diffraction pattern of concentric rings from an approximately spherical plasma with $N \approx 7.5 \times 10^5$. Even if this pattern is from a single crystal, rings are observed because of the plasma rotation about the axial laser beam [4]. With the rotating field applied and controlling the plasma rotation, we trigger the intensifier synchronously with the rotating field to open the camera for 50 ns each $2\pi/\omega_w$ period. This enables the camera to record the diffraction pattern in the rest frame of the rotating field. Figure 3(b) shows such a time-resolved pattern taken nearly simultaneously with Fig. 3(a) and accumulated over $\sim 10^6$ plasma rotations. The well-defined rectangular dot pattern demonstrates that the crystal is phase locked to the rotating field. This phase-locked rotation is routinely obtained when $\mathbf{B_0}$ is aligned within 0.01° of the trap axis. In addition, the crystalline lattice and its orientation with respect to the laser beam can last longer than 30 min under this rotation control.

With the rotating quadrupole field, the plasma surface is actually a spinning triaxial ellipsoid with three principal axes differing in length [17]. This particular shape results in a total electric field having only the radial component so that the plasma undergoes a purely azimuthal motion with a uniform rotation frequency. Since $\omega_r = \omega_w$, the combined vacuum trapping potential in the rotating frame becomes $\Phi_r' = (m\omega_z^2/2e)[z^2 + (\beta - \delta)x_r^2 + (\beta + \delta)y_r^2]$, where $\delta = f_g V_w/V_0 \geq 0$ is the relative strength of the rotating field and f_g depends only on the trap geometry. The thermal equilibrium state in the frame rotating with the plasma is bounded by $z^2/z_0^2 + x_r^2/x_0^2 + y_r^2/y_0^2 = 1$ with $x_0 \geq y_0$, and the parallel and perpendicular aspect ratios ($\alpha_\parallel \equiv z_0/y_0, \alpha_\perp \equiv x_0/y_0$) are determined by β and δ [17].

To maximize δ/β, we reduce V_0 to less than 200 V and set ω_w close to ω_m. Side-view images of the plasma are obtained at different phases of the rotating field. In the laboratory frame, the plasma radius along the x axis is expected to oscillate at $2\omega_w$, with an amplitude proportional to $x_0 - y_0$. Figure 4 shows such a plasma with $\alpha_\parallel \approx 0.15$ and $\alpha_\perp \approx 1.4$ rotating at 2.5 kHz ($V_0 = 50$ V,

$V_w \approx 185\,\mathrm{V}$). Excellent agreement between the theory and data is exhibited, showing that the plasma is indeed equilibrated with the rotating field.

We have measured the dependence of $\alpha_\perp$ on parameters δ and β. Figure 5(a) shows $\alpha_\perp$ versus δ at fixed $\beta = 0.103$. Good agreement with the theory is obtained by fitting this data for f_g with the result $f_g \approx 6.38 \times 10^{-3}$. Figure 5(b) shows $\alpha_\perp$ versus β for fixed $\delta \approx 0.0159$ using the calibrated f_g value. Excellent agreement is again observed, showing the rapid decrease to unity for $\alpha_\perp$ as β is increased. Under typical conditions ($V_0 \geq 500\,\mathrm{V}$, $V_w \leq 50\,\mathrm{V}$, and $\omega_w \geq 1.1\omega_m$, giving $\delta < 7 \times 10^{-4}$ and $\beta > 0.1$), $\alpha_\perp - 1$ is less than 1 %, but this small distortion apparently generates sufficient torque to phase lock the plasma rotation.

We have also examined rotation control using the dipole field with a potential $\propto y\sin(\omega_w t) - x\cos(\omega_w t)$. Theoretically, this field should not control the plasma rotation, because for a single-species plasma in a quadratic trap it only causes a center-of-mass orbital motion about the trap axis and is thus decoupled from the internal plasma rotation. Experimentally, phase-locked rotation control similar to that by the quadrupole field is obtained. In addition, because larger dipole fields can be applied, rotation stabilization in the range $\omega_m < \omega_r \lesssim 0.9\,(\Omega - \omega_m)$, which includes the Brillouin flow, has been achieved. Experimental evidence suggests that the coupling between the center-of-mass motion and plasma rotation can be provided by the contaminant ions which have a slightly larger center-of-mass displacement than $^9Be^+$ due to centrifugal inertia. By measuring the plasma dynamic response under sudden change of ω_w [15], we have observed that the torque from the dipole field increases with time, presumably due to the growing number of contaminant ions. This observation, however, does not exclude the possibility that other non-ideal effects can also provide the coupling.

In the future, direct imaging of individual ions in a crystallized plasma may be possible because of the phase-locked rotation. Furthermore, the increased crystal stability improves the prospect of observing the solid–liquid phase transition.

We thank D. Wineland, D. Dubin, T. O'Neil, and C.F. Driscoll for discussions; B. Jelenković, J. Tan, J. Bergquist, and L. Hollberg for technical assistance; and D. Leibfried, C. Myatt, M. Young, and D. Sullivan for useful comments. This work is supported by the Office of Naval Research.

[1] J.H. Malmberg, C.F. Driscoll, B. Beck, D.L. Eggleston, J. Fajans, K. Fine, X.-P. Huang, and A.W. Hyatt, in *Non-neutral Plasma Physics*, edited by C.W. Roberson and C.F. Driscoll (AIP, New York, 1988), p. 28.

[2] J.J. Bollinger, D.J. Wineland, and D.H.E. Dubin, Phys. Plasmas **1**, 1403 (1994).

[3] T.M. O'Neil, Phys. Fluids **23**, 2216 (1980).

[4] J.N. Tan, J.J. Bollinger, B. Jelenkovic, and D.J. Wineland, Phys. Rev. Lett. **75**, 4198 (1995); J.N. Tan, J.J. Bollinger, B. Jelenkovic, W.M. Itano, and D.J. Wineland, in *Physics of Strongly Coupled Plasmas*, edited by W.D. Kraeft and M. Schlanges (World Scientific, Singapore, 1996), p. 387.

[5] W.M. Itano, J.J. Bollinger, J.N. Tan, B. Jelenkovic, X.-P. Huang, and D.J. Wineland, "Bragg Diffraction from Crystallized Ion Plasmas", submitted to Science (1997).

[6] R. Blatt, P. Gill, and R.C. Thompson, J. Mod. Optics **39**, 193 (1992); R.C. Thompson, Adv. At. Mol. Phys. **31**, 63 (1993).

[7] J.N. Tan, J.J. Bollinger, and D.J. Wineland, IEEE Trans. Instrum. Meas. **44**, 144 (1995).

[8] G. Savard, St. Becker, G. Bollen, H.-J. Kluge, R.B. Moore, Th. Otto, L. Schweikhard, H. Stolzenberg, and U. Wiess, Phys. Lett. A **158**, 247 (1991); S. Guan, X. Xiang, and A.G. Marshall, Int. J. Mass Spec. Ion Proc. **124**, 53 (1993).

[9] F. Anderegg, X.-P. Huang, C.F. Driscoll, E.M. Hollmann, T.M. O'Neil, and D.H.E. Dubin, Phys. Rev. Lett. **78**, 2128 (1997).

[10] G. Gabrielse, X. Fei, L.A. Orozco, R.L. Tjoelker, J. Hass, H. Kalinowsky, T.A. Trainer, and W. Kells, Phys. Rev. Lett. **65**, 1317 (1990).

[11] R.G. Greaves and C.M. Surko, Phys. Plasmas **4**, 1528 (1997).

[12] D. Schneider, D.A. Church, G. Weinberg, A.J. Steiger, B. Beck, J. McDonald, E. Magee, and D. Knapp, Rev. Sci. Instrum. **65**, 3472 (1994).

[13] J.J. Bollinger and D.J. Wineland, Phys. Rev. Lett. **53**, 348 (1984).

[14] L.R. Brewer, J.D. Prestage, J.J. Bollinger, W.M. Itano, D.J. Larson, and D.J. Wineland, Phys. Rev. A **38**, 859 (1988); D.J. Heinzen, J.J. Bollinger, F.L. Moore, W.M. Itano, and D.J. Wineland, Phys. Rev. Lett. **66**, 2080 (1991).

[15] X.-P. Huang, F. Anderegg, E.M. Hollmann, C.F. Driscoll, and T.M. O'Neil, Phys. Rev. Lett. **78**, 875 (1997).

[16] Preliminary results on pure electron plasmas are in R.E. Pollock and F. Anderegg, in *Non-neutral Plasma Physics II*, edited by J. Fajans and D.H.E. Dubin (AIP, New York, 1995), p. 139.

[17] D.H.E. Dubin and T.M. O'Neil, "Trapped Non-neutral Plasmas, Liquids, and Crystals (the Thermal Equilibrium States)", submitted to Rev. Mod. Phys. (1997).

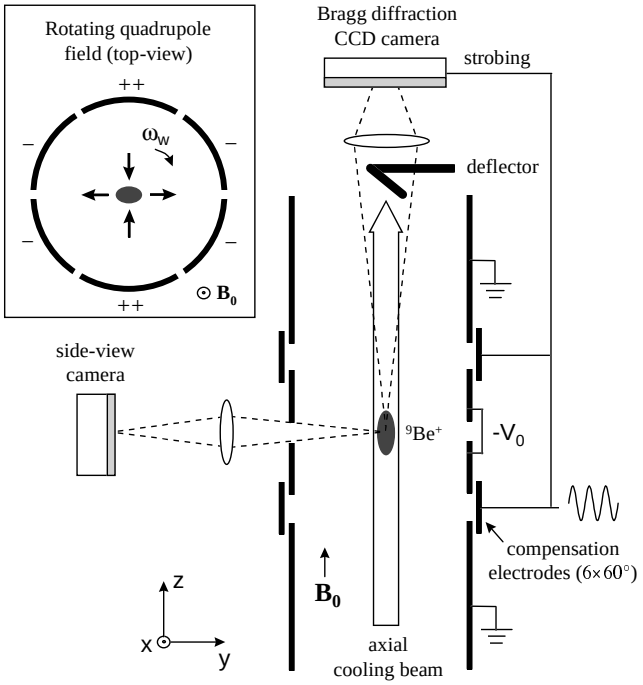

FIG. 1. Schematic side-view of the cylindrical trap with real-space imaging optics and Bragg diffraction detection system. Cross section of the rotating quadrupole field (in the x-y plane) is shown in the inset.

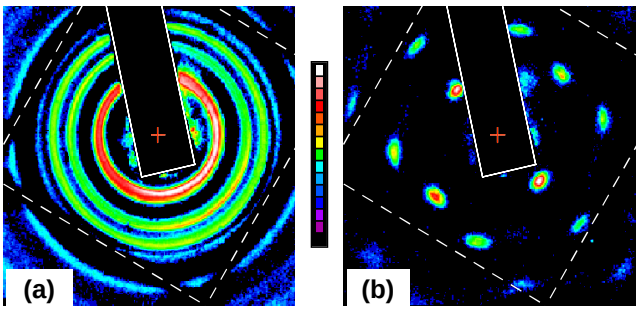

FIG. 3. Bragg diffraction from a crystalline lattice (bcc with a {110} plane $\perp$ to z axis) in a plasma phase locked to the rotating field ($\omega_r = \omega_w = 2\pi \times 140\,\mathrm{kHz}$, $n_0 \approx 4.3 \times 10^8\,\mathrm{cm}^{-3}$, $\alpha \approx 1.1$). (a) 1 s time-averaged pattern; (b) Time-resolved pattern by strobing the camera with the rotating field (integration time ≈ 5 s). Both graphs are in false-color with logarithmic photon count scales. The long rectangular shadow is from the deflector for the incident beam; four line shadows that form a square are due to a wire mesh at the exit window of the vacuum chamber.

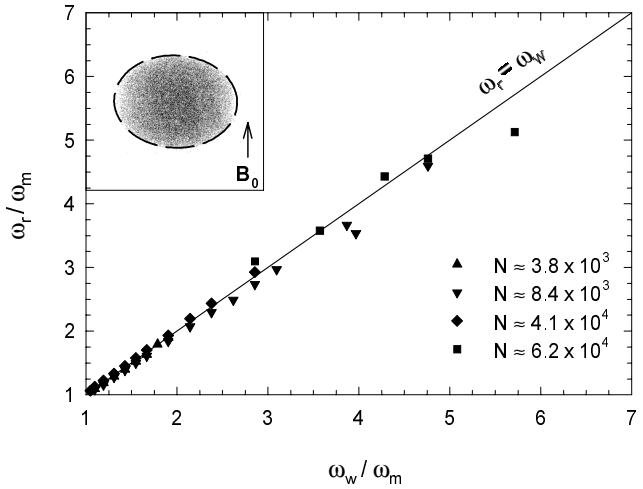

FIG. 2. The plasma rotation frequency ω_r versus the quadrupole field rotation frequency ω_w. The frequency ω_r is determined from the aspect ratio α of several plasmas with $200 \le V_0 \le 500\,\mathrm{V}$. The inset shows a typical side-view image and its boundary fit to an ellipse (dashed line), giving α and ω_r.

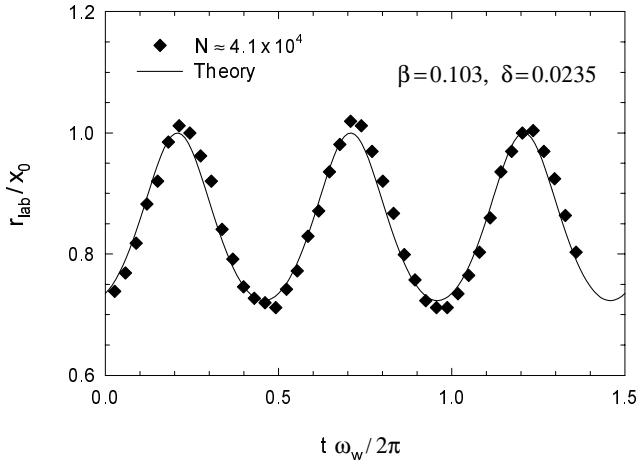

FIG. 4. Oscillation of the plasma radius r_{lab} in 1.5 rotation periods. The theory curve is calculated using the calibrated f_g from Fig. 5(a). The relative phase between the theory and data is not adjusted.

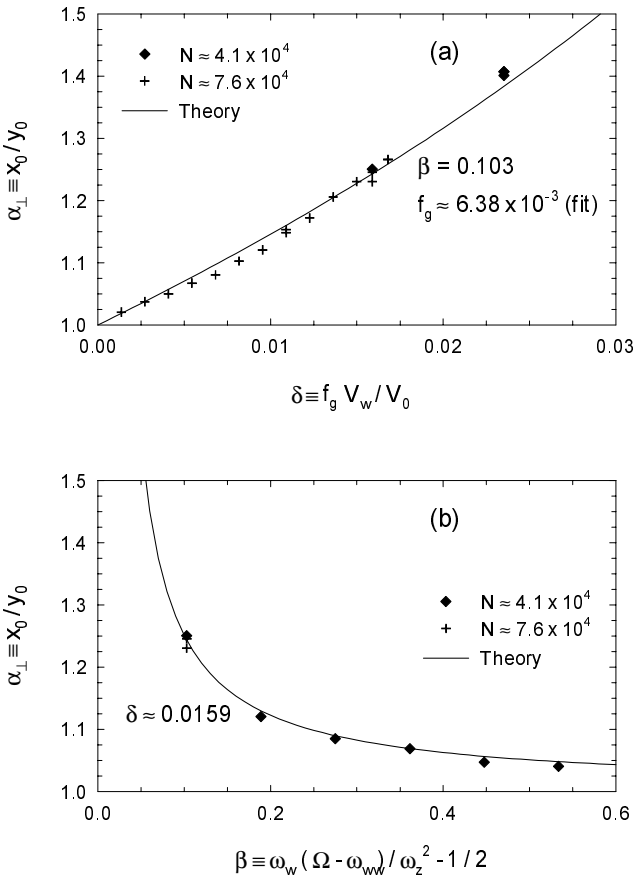

FIG. 5. Dependence of perpendicular aspect ratio $\alpha_\perp$ versus (a) rotating field strength δ and (b) radial trapping strength β. Two plasmas are used with $50 \leq V_0 \leq 100\,\mathrm{V}$ and $15 \leq V_w \leq 185\,\mathrm{V}$. The geometric factor f_g is calibrated in (a).